Proceedings of SPIE Conference on Remote Sensing of the Ocean and Sea Ice, Barcelona, Spain
September 8-12, 2003

Validation of Wavewatch-III Using the TOPEX/POSEIDON Data

Peter C. Chu [1)], Yiquan Qi [2)], Yuchun Chen[3)], Ping Shi[2)], and Qingwen Mao[2)]

[1)] Naval Ocean Analysis and Prediction Laboratory, Department of Oceanography
Naval Postgraduate School, Monterey, CA 93943, USA
[2)] South China Sea Institute of Oceanology, Guangzhou, China
[3)] Cold and Arid Regions Environmental and Engineering Research Institute, Lanzhou, China

ABSTRACT

A full-spectral third-generation ocean wind-wave model, Wavewatch-III, has been implemented in the South China Sea (SCS) for investigating the wind wave characteristics. This model was developed at the Ocean Modeling Branch of the National Centers for Environmental Prediction (NCEP). The NASA QuickScat data (0.25^o resolution) two times daily were used to simulate the wind waves for the whole year in 2000. The significant wave heights from Wavewatch-III are compared to the TOPEX/POSEIDON (T/P) significant wave height data over the satellite crossover points in SCS. The model errors of significant wave height have Gaussian-type distribution with small mean value of 0.02 m (almost no bias). The model errors are comparable to the T/P altimeter accuracy (0.5 m) in the central SCS and smaller than the T/P altimeter accuracy in the northern and southern SCS, which indicates the capability of Wavewatch-III for SCS wave simulation.

Keywords: TOPEX/POSEIDON altimetry, QuikSCAT winds, Wavewatch-III, significant wave height, wave action spectrum

1. INTRODUCTION

A fully spectral third-generation ocean wind-wave model, Wavewatch-III (henceforth denoted as WWATCH), has been recently developed at the Ocean Modeling Branch of the Environmental Modeling Center of the National Centers for Environmental Prediction (NCEP) for the regional sea wave prediction. It was built on the base of Wavewatch-I and Wavewatch-II as developed at the Delft University of Technology, and NASA Goddard Space Flight Center, respectively (Tolman 1999). WWATCH should be evaluated before the practical use.

The South China Sea (SCS) is a semi-enclosed tropical sea located between the Asian land mass to the north and west, the Philippine Islands to the east, Borneo to the southeast, and Indonesia to the south (Fig. 1), a total area of $3.5 \ 10^6$ km^2. It connects to the East China Sea (through Taiwan Strait), the Pacific Ocean (through Luzon Strait), the Sulu Sea, the Java Sea (through Gasper and Karimata Straits), and to the Indian Ocean (through the Strait of Malacca). All of these straits are shallow except Luzon Strait whose maximum depth is 1800 m. The elliptical shaped central deep basin is 1900 km along its major axis (northeast-southwest) and approximately 1100 km along its minor axis, and extends to over 4000 m deep.

The SCS is under the influence of monsoon winds and synoptic systems such as fronts and tropical cyclones. From November to March, the northeasterly winter monsoon winds correspond to monthly mean January 2000 wind speeds of near 10 m/s for the whole SCS (Fig. 2a). From April to August, the southwesterly summer monsoon winds result in a

monthly mean July 2000 wind speeds of approximate 8 m/s in the Southern SCS and 4 m/s in the northern SCS (Fig. 2b). The monthly mean winds (Fig. 2) are typical for monsoon winds. Highly variable winds and surface currents are observed during the transitional periods. Moreover, synoptic systems often pass by the SCS and causes temporally and spatially varying wind fields.

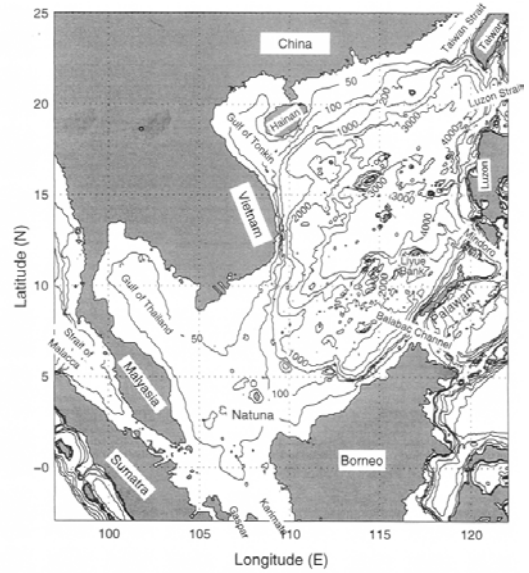

Figure 1. Geography and isobaths showing the bottom topography of the South China Sea.

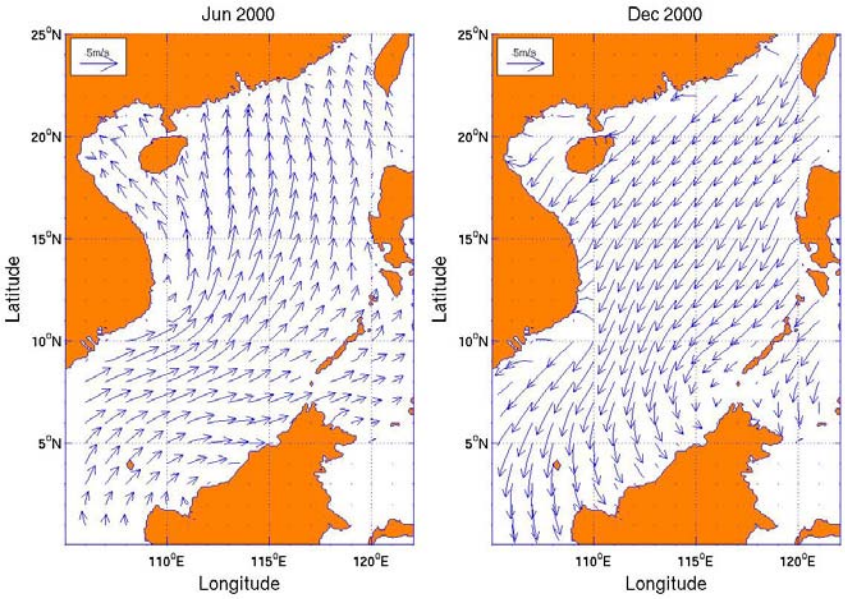

Fig. 2. Monthly mean wind speed at 10 m height computed from the QSCAT data: (a) January 2000, and (b) July 2000.

The highly variable wind systems and complicated topography make SCS a perfect location for WWATCH evaluation. Usually the in-situ wind wave data are mainly collected from voluntary ships and wave buoys. However, in SCS sparse voluntary ship data and no wave buoy data are available. This makes the remote sensing be an important source for the wind wave data. Several satellites have been launched with altimetry, such as TOPEX/POSEIDON (T/P), ERS-1/2. The subsequent sections describe the WWATCH evaluation using the T/P significant wave height (SWH) data.

2. T/P DATA

The T/P satellite, jointly launched by NASA and the French Space Agency, the Center National d'Etudes Spatiales (CNES) in August 1992, carried a state-of-the-art radar altimetry system (Fu et al. 1994). In addition to precise measurements of the distance between the satellite and the surface, SWH was derived from the shape of the leading edge of the returning radar pulse. The accuracy of SWH measurement by T/P was within the accuracy of the Geosat measurements (Callahan et al. 1994), i.e., 10% or 0.5 m, whichever is greater (Dobson et al. 1987). T/P was maneuvered into a 9.9156-day repeat period during which two T/P SWH data are available at each crossover point. Time series of SWH at 20 crossover points shown in Fig. 3a and 4 passes (051, 229, 152, 190) shown in Fig. 3b for 2000 are used to evaluate WWATCH.

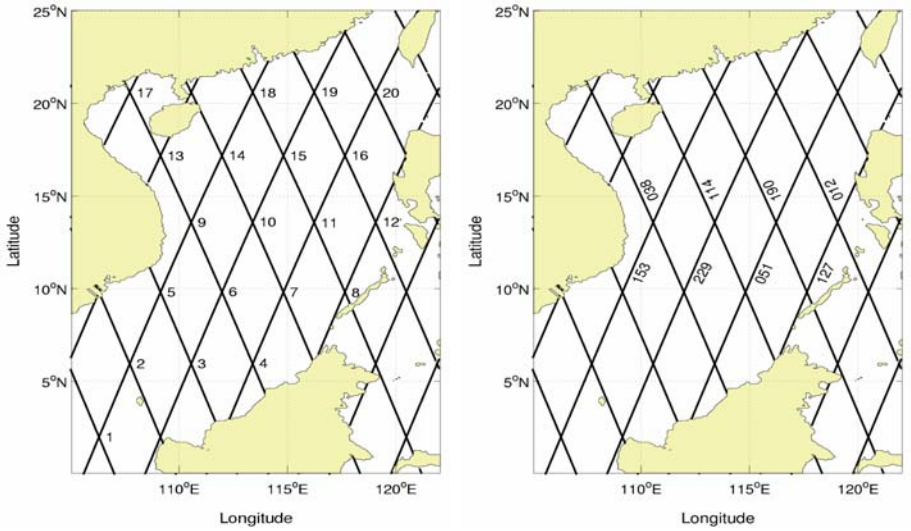

Fig.3. T/P (a) crossover points and (b) tracks in the SCS.

3. WWATCH MODEL

The wave spectrum F is generally a function of all phase parameters (i.e., wave number k, direction , intrinsic frequency σ, and absolute frequency ω), space ($\mathbf{x}$), and time (t),

$$F = F(k, \ , \sigma, \omega; \mathbf{x}, t).$$

However, the individual spectral components are usually assumed to satisfy the linear wave theory (locally) and to follow the dispersion relation with Doppler effect,

$$\sigma^2 = gk \tanh kd \qquad (1)$$

$$\omega = \sigma + \mathbf{k}\ \mathbf{U} \qquad (2)$$

where d is the mean water depth and $\mathbf{U}$ is the (depth- and time- averaged) current velocity. When the current velocity vanishes, only two-phase parameters among (, k,) are independent. Current wave models use the frequency-direction (,) as the independent phase variables.

WWATCH uses the wavenumber-direction (k,) as the independent phase variables. Without currents, the energy of a wave package is conserved. With currents the energy of a spectral component is no longer conserved (Longuet-Higgins et al. 1961), but the wave action spectrum, $N(k,\theta; \mathbf{x}, t)$ $F(k,\theta; \mathbf{x}, t)/$, is conserved (Whitham 1965; Bretherthon and Garrett 1968). In WWATCH, the balance equation is for the wave action spectrum. The model setting for this study is given in Table 1.

The surface winds ($\boldsymbol{U}$) for the year of 2000 are obtained from the NASA SeaWinds on twice daily QuikScat (QSCAT) Level-3 gridded ocean wind vectors with 0.25° horizontal resolutions. The friction velocities are needed for the input source function S_{in}. In WWATCH, the friction velocity (u_*) is computed from the wind speed (U) at a given reference height z_{r}, in terms of a drag coefficient C_r (Tolman and Chalikov 1996).

WWATCH is integrated with twice daily NASA SeaWinds on QSCAT level-3 gridded ocean wind vectors (0.25°) from the JONSWAP 1973 wave spectra (Hasselmann et al. 1980) on January 3 (no sufficient wind data on January 1-2, 2000 for SCS), 2000 until 31 December 2000. The model SWH data are interpolated into the T/P crossover points, where the hindcast and altimeter wave heights are compared. At each crossover point, there are M pairs (approximately 72) of modeled (H_{m}) and observed (H_{o}) SWH data in 2000 (around 2 pairs per 10 days).

Table 1. Model setting for this study.

Switch Parameters	Characteristics
DUM	Dummy to be used if WWATCH is to be installed on previously untried hardware
LRB8	8 byte words
SHRD	Shared memory model, no message passing
SEED	Seeding of high-frequency energy
GRD1	Settings directly hardwired to user-defined spatial grids (spherical coordinate with 0.25$^{\text{o}}$ grids)
SP1	Use-defined spectral grids.
PR2	Ultimate quickest propagation scheme with Booij and Holthuijsen (1987) dispersion correction
ST2	Tolman and Chalikov (1996) source term package
STAB2	Enable stability correction for Tolman and Chalikov (1996) source term package
NL1	Nonlinear interaction (DIA)
BT1	JONSWAP bottom friction formulation
WIND2	Approximately quadratic interpolation
CUR2	Approximately quadratic interpolation
o1	Output of boundary points in grid preprocessor
o2	Output of the grid point status map in grid preprocessor
o2a	Generation of land-sea mask file mask.ww3 in grid preprocessor
o3	Additional output in loop over fields in field preprocessor
o4	Print plot of normalized 1-D energy spectrum in initial conditions program
o5	2-D energy spectrum
o6	Spatial distribution of wave heights (not adapted for distributed memory)
o7	Echo input data for homogeneous fields in generic shell

4. METHODOLOGY OF VERIFICATION

4.1. Verification at Crossover Points

The difference of the modeled and observed SWH,

$$H = H_m(x, y, t) - H_o(x, y, t) \tag{3}$$

represents the model error. Bias, root-mean-square error (rmse), and correlation coefficient (cc) for each crossover point

$$\text{bias}(x, y) = \frac{1}{M}\sum_{i=1}^{M}\Delta H(x, y, t_i), \tag{4}$$

$$\text{rmse}(x, y) = \sqrt{\frac{1}{M}\sum_{i=1}^{M}\left[\Delta H(x, y, t_i)\right]^2}, \tag{5}$$

$$\text{cc}(x, y) = \frac{\sum_{i=1}^{M}\left[(H_m(x, y, t_i) - \bar{H}_m(x, y)\right]\left[(H_o(x, y, t_i) - \bar{H}_o(x, y)\right]}{\sqrt{\sum_{i=1}^{M}\left[(H_m(x, y, t_i) - \bar{H}_m(x, y)\right]^2}\sqrt{\sum_{i=1}^{M}\left[(H_o(x, y, t_i) - \bar{H}_o(x, y)\right]^2}}, \tag{6}$$

are used to verify WWATCH. Here $\bar{H}_m(x, y)$ and $\bar{H}_o(x, y)$ are temporal mean modeled and observed SWH,

$$\bar{H}_m(x, y) = \frac{1}{M}\sum_{i=1}^{M}H_m(x, y, t_i), \quad \bar{H}_o(x, y) = \frac{1}{M}\sum_{i=1}^{M}H_o(x, y, t_i), \tag{7}$$

at the crossover points. The significant test of cc is conducted using *T*-value constructed by

$$T = \frac{\text{cc}\sqrt{\text{M-2}}}{\sqrt{1\text{-cc}^2}}, \tag{8}$$

with the degree of freedom of (M - 2).

4.2. Verification at Time Instance

Bias and rmse for time instance *t*

$$\text{bias}(t) = \frac{1}{N}\sum_{j,k}\Delta H(x_j, y_k, t), \tag{9}$$

$$\text{rmse}(t) = \sqrt{\frac{1}{N}\sum_{j,k}\left[\Delta H(x_j, y_k, t)\right]^2}, \tag{10}$$

are also used to verify WWATCH.

5. MONTHLY MEAN SWH

Three sets of monthly mean data (averaged from twice daily data) are used for the evaluation: (a) modeled SWH from WWATCH, (b) calculated SWH from the Pierson-Moskowitz (P-M) spectrum (1964) using the same QSCAT winds, and (c) observed SWH from T/P. A common feature is found among the simulated (Fig. 4), calculated (Fig. 5), and observed (Fig. 6) data that the mean SWHs are higher in January (2000) than in July (2000).

In January (2000), a southwest to northeast oriented high SWH region (> 2.0 m) is comparable (north of 5^o N) in the WWATCH simulation (Fig. 4a) and in the T/P data (Fig. 6a). However, this high SWH region is split into two

smaller ones in the calculated (from P-M spectrum) field with a major one occurring north of 15°N and a minor one near the southern Vietnamese coast (Fig. 5a). The area with SWH larger than 2.5 m in the WWATCH simulation (113°–117°E, 15°–20°N) is comparable to that in the T/P data (112°–1117°E, 13°–20°N).

In July (2000), the mean SWHs are higher in the northern and central SCS (north of 10°N) than in the southern SCS (south of 10°N) with values larger than 2.25 m in the WWATCH simulated field (Fig. 4b) and than 2.5 m in the observed fields (Fig. 5b). However, the maximum SWH values are located at (115°-120°E, 11°-15°N) in simulated and calculated fields and at (113°-116°E, 15°-20°N) in the observed field. WWATCH simulates the seasonal variability of SWH reasonably well. SWH is larger in the winter than in the summer monsoon season. The orientation of the high SWH region coincides with the orientation of the monsoon winds (Fig. 2).

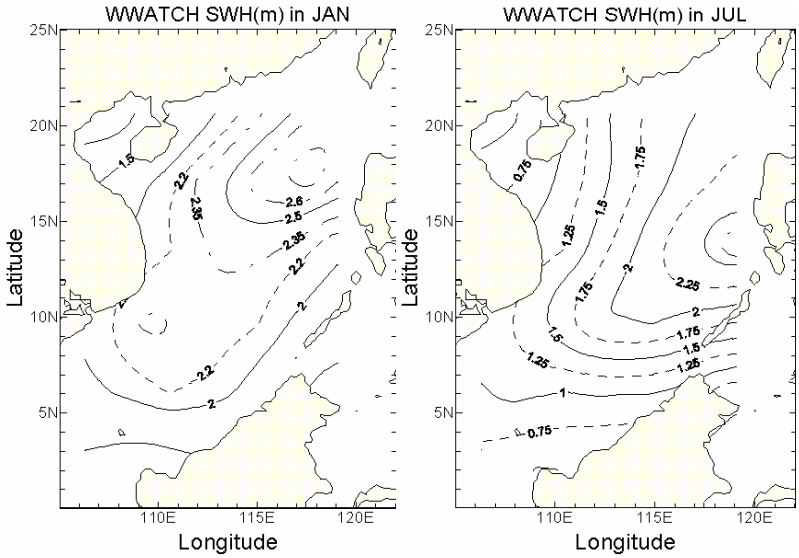

Fig. 4. Predicted monthly mean SWH using WWATCH (a) January, and (b) July, 2000.

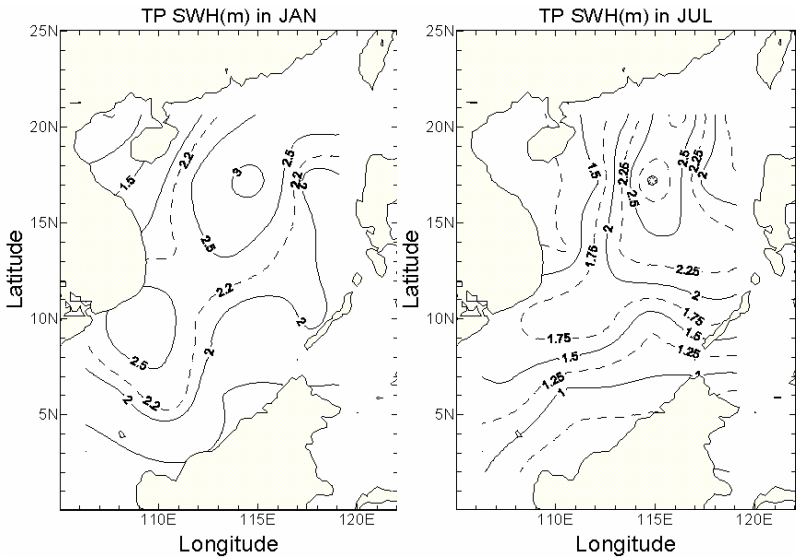

Fig. 5. Monthly mean SWH from T/P data (a) January, and (b) July, 2000.

6. STATISTICAL EVALUATION

The histogram of H (Fig. 7a) for all the crossover points in the SCS shows a Gaussian-type distribution with mean value (0.02 m) and with comparable sample number of positive H (633) with negative H (697). The scatter diagrams for H_m and H_o show clustering of points approximately around the line of $H_m = H_o$ (Fig. 7b). The rmse and cc between H_m and H_o are 0.48 m and 0.90.

The scatter diagrams for H_m and H_o at each crossover points (Fig. 8) show spatial variability of the error statistics. The rmse varies from 0.34 m at Point #1 (106.31°E, 2.01°N) to 0.95 m at Point #15 (114.81°E, 17.18°N) and Point #16 (117.65°E, 17.20°N). The bias varies from -0.45 m at Point #17 (107.73°E, 20.59°N) to 0.33 m at Point #7 (114.81°E, 9.8°N). The correlation coefficients vary from 0.55 at Point #17 (107.73°E, 20.59°N) to 0.95 at Point #15 (114.81°E, 17.18°N).

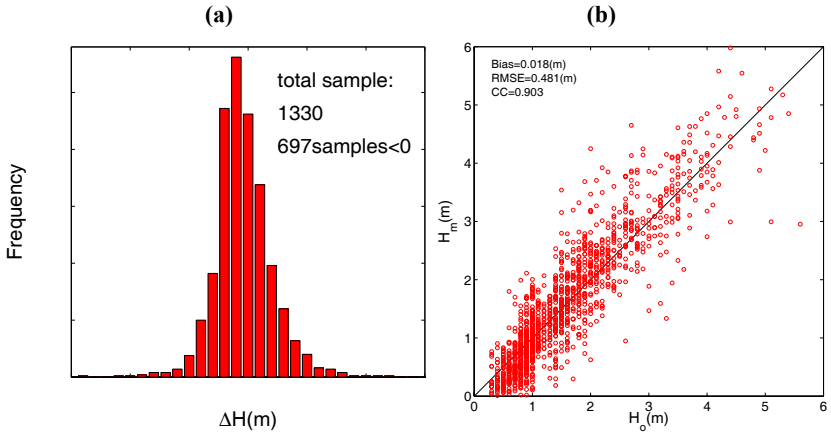

Fig 6. Model accuracy statistics: (a) histogram of model error, and (b) scatter diagram of modeled (H_m) and observed (H_o) SWH for all the crossover points.

Contours of bias, rmse, and cc for the whole year (2000) are plotted (Fig. 7) to understand the spatial error variability. The positive bias occupies large portion of the SCS. The zero-bias contour follows 200-m bathymetry (Fig. 1) with negative bias on the continental shelf (west of the zero-bias contour) and positive bias in the deep basin (east of the zero-bias contour). The negative bias larger than –0.4 m is found in the Gulf of Tokin and the positive larger than 0.3 m is located near Nansha Island (115°E, 10°N) (Fig. 7a). This indicates that WWATCH-SCS overpredicts the SWH slightly except on the shallow continental shelf. The rmse of SWH is above 0.5 m in the central SCS with a maximum larger than 0.6 m west of Palawan (Fig. 9b). The value of rmse decreases from the central SCS to the other two regions, and is smaller than 0.5 m in most of northern (west of Luzon) and southern (south of 5°N) SCS.

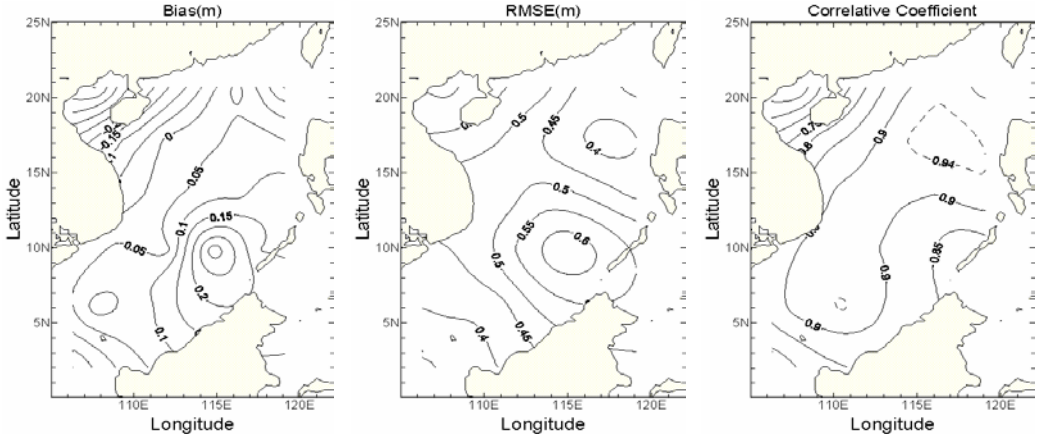

Fig. 7. Distributions of SWH (a) bias, (b) rms error, and (c) correlation coefficient between WWATCH and T/P data.

The cc of SWH (Fig. 7c) between modeled and T/P data in 2000 is larger than 0.85 almost everywhere in SCS except in the Gulf of Tonkin. The T-value computed using (8) for cc = 0.85, M = 72 is: $T = 13.50$. For confidence coefficient $(1 - \alpha) = 0.095$, the t-distribution for the degree of freedom of statistics for (M - 2 = 70) is: $2.756 > t_{0.005} > 2.576$. Since T (= 13.50) is larger than $t_{0.005}$, the correlation coefficient between modeled and T/P SWH data is significant.

7. TEMPORAL ERROR VARIABILITY

The monthly mean bias and rmse averaged over all the crossover points in the SCS are presented (Fig. 8) to represent the temporal error variability for the whole SCS. WWATCH-SCS has very low bias (-0.01 to 0.04 m) in predicting SWH with a maximum (positive bias) value of 0.04 m in March and a minimum (negative bias) value of –0.01 m in April. The rmse has a minimum value of 0.39 m in March and a maximum value of 0.48 m in December.

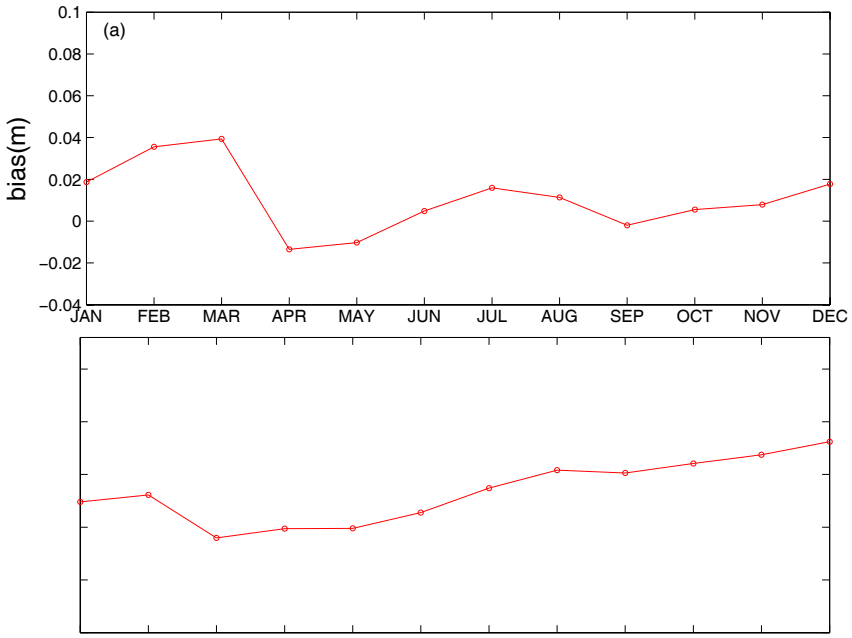

Fig. 8. Temporal evolution of (a) bias and (b) rmse for the whole SCS.

8. CONCLUSIONS

Comparing the South China Sea significant wave height hindcast using the third generation wave model (Wavewatch-III) with significant wave height measured by TOPEX/POSEIDON altimeter for 2000, several characteristics of the model errors are obtained for the three subregions: central, northern, and southern SCS.

(1) Wavewatch-III simulates the seasonal variability of SWH reasonably well comparing to the T/P SWH data. July (2000) SWHs are higher in the northern and central SCS (north of 10°N) than in the southern SCS (south of 10°N) with values larger than 2.25 m in the WWATCH simulated field and than 2.5 m in the calculated (from the Pierson-Moskowitz spectrum) and observed fields. The orientation of the high SWH region coincides with the orientation of the monsoon winds.

(2) The model errors for SWH hindcast have Gaussian-type distribution with mean values of 0.02 m and with slightly more sample number on the negative side (697) than on the positive side (633). The root-mean-square error and correlation coefficient between modeled and observed significant wave heights are 0.48 m and 0.90.

(3) The model errors of WWATCH-SCS have spatial variability with overprediction of the SWH except on the shallow continental shelf. The rmse of SWH is above 0.5 m in the central SCS with a maximum larger than 0.6 m west of Palawan. The value of rmse northward and southward decreases from the central SCS, and is smaller than 0.5 m in most of northern (west of Luzon) and southern (south of 5^{o}N) SCS.

(4) Over the whole SCS, WWATCH has very low bias (-0.01 to 0.04 m) in predicting SWH with a maximum (positive bias) value of 0.04 m in March and a minimum (negative bias) value of –0.01 m in April. The root-mean-square error has a minimum value of 0.39 m in March and a maximum value of 0.48 m in December.

(5) The model errors are comparable to the T/P altimeter accuracy (0.5 m) in the central SCS and smaller than the T/P altimeter accuracy in the northern and southern SCS, which indicates the capability of Wavewatch-III for SCS wave simulation.

ACKNOWLEDGMENTS

The authors wish to thank Dr. Tolman at the National Weather Service for providing the Wavewatch-III model, the NOAA-CIRES Climate Diagnostics Center for providing NCEP Reanalysis data, and NASA/JPL for providing TOPEX/POSEIDON data. This work was jointly funded by the Naval Oceanographic Office, the Naval Postgraduate School, the Chinese Academy of Sciences (Project KZCX2-202), the National Natural Science Foundation of China (49976006), and the Science Foundation of Guangdong Province, China (990314).

REFERENCES

Bao, J.-W., J.M. Wilczak, J.-K. Choi, and L.H. Kantha, 2000: Numerical simulation of air-sea interaction under high wind conditions using a coupled model: A study of hurricane development. Mon. Wea. Rev., 128, 2190-2210.

Booij, N., and L.H. Holthuijsen, 1987: Propagation of ocean waves in discrete spectral wave models. J. Comput. Physics, 68, 307-326.

Bretherthon, F.P., and C.J.R. Garrett, 1968: Wave trains in inhomogeneous moving media. Proc. Roy. Soc. London, A 302, 529-554.

Callahan, P.S., C.S. Morris, and S.V. Hsiao, 1994: Comparison of TOPEX/POSEIDON $_0$ and significant wave height distributions to Geosat. J. Geophys. Res., 99, 25015-25024.

Chen, S.S., W. Zhao, J. E. Tenerelli, and M. Donelan, 2002: Atmosphere-wave-ocean coupling in tropical cyclones. 25th Conference on Hurricanes and Tropical Meteorology, Orlando, FL, April 28 - May 3, 2002.

Dobson, E., F. Monaldo, and J. Goldhirsh, 1987: Validation of Geosat altimeter-derived wind speeds and significant wave heights using buoy data, J. Geophys. Res., 92, 10719-10731.

Fu, L.L., E. J. Christensen, C.A. Yamaone Jr., M. Lefebvre, Y. Menard, M. Dorrer, and P. Escudier, 1994: TOPEX/POSEIDON mission overview. J. Geophys. Res., 99, 24369-24381.

Hasselmann, D.E., M. Dunckel, and J.A. Ewing, 1980: Directional wave spectra observed during JONSWAP 1973. J. Phys. Oceanogr., 10, 1264-1280.

Janssen, P.A.E.M., 1989: Wave-induced stress and the drag of air flow over sea waves. J. Phys. Oceanogr., 19, 745-754.

Longuet-Higgins, M. S., and R. W. Stewart, 1961: The changes in amplitude of short gravity waves on steady non-uniform currents. J. Fluid Mech., 10: 529-549.

Shemdin, O., K. Hasselmann, S. V. Hsiao and K. Heterich, 1978: Nonlinear and linear bottom interaction effects in shallow water, in : Turbulent fluxes through the sea surface, wave dynamics and prediction. NATO Conf. Ser. V, Vol. 1, 347-365.

Tolman, H.L, 1999: User manual and system documentation of WAVEWATCH-III version 1.18, NOAA/NCEP Technical Note 166, pp. 110.

Tolman, H.L. and D.V. Chalikov, 1996: Source terms in a third-generation wind wave model. J. Phys. Oceaogr., 26:2497-2518.

Tolman, H.L. and N. Booij, 1998: Modeling wind waves using wavenumber-direction spectra and a variable wavenumber grid. Global atmosphere and ocean system. 295-309.

Whitham, G.B., 1965: A general approach to linear and non-linear dispersive waves using a Lagrangian. J. Fluid Mech., 22:273-283.